RSC Advances

ROYAL SOCIETY OF CHEMISTRY

www.rsc.org/advances

RSC Advances

ARTICLE

Enhancing visible-light photocatalytic activity of g-C_3N_4 by doping phosphorus and coupling with CeO_2 for the degradation of methyl orange under visible light irradiation †

Received 00th January 2015,
Accepted 00th January 2015

DOI: 10.1039/x0xx00000x

www.rsc.org/

Jin Luo,* Xiaosong Zhou, Lin Ma, Xuyao Xu

CeO_2/P-C_3N_4 composite photocatalysts were designed by doping phosphorus and coupling with CeO_2 species. The structure and optical properties of the as-prepared samples were characterized by scanning electron microscopy, transmission electron microscopy, X-ray diffraction, X-ray photoelectron spectroscopy, UV-vis diffuse reflectance spectroscopy and photoluminescence spectroscopy. The photocatalytic activity of the CeO_2/P-C_3N_4 was evaluated by photocatalytic degradation of methyl orange (MO) under visible light irradiation (λ>420 nm). The results indicated that the optimum photocatalytic activity of CeO_2/P-C_3N_4 at a weight content of 13.8% CeO_2 for the degradation of MO was 7.4 and 4.9 times as high as that of pure CeO_2 and g-C_3N_4, respectively. The remarkable enhancement of photocatalytic activity could be attributed to the synergistic effect between CeO_2 and P-C_3N_4, which was found to extend the visible light absorption range, enhance visible light absorption and improve photogenerated electron-hole pairs separation efficiency after doping phosphorus and coupling with CeO_2. Additionally, the superoxide radical anions ($\bullet O_2^-$) and holes (h^+) were considered as the main reactive species during the photodegradation MO process, and a possible photocatalytic mechanism over CeO_2/P-C_3N_4 composite photocatalyst was proposed based on the experimental results.

Introduction

Semiconductor photocatalysis has received a great deal of attention due to it represents a promising alternative technology for degradation of organic pollutants and hydrogen production from splitting water.[1] During the past few decades, TiO_2 semiconductor is considered as one of the most promising photocatalyst and has been extensively investigated owing to the non-toxicity, low cost, relatively high chemical stability and strong oxidizing power.[2] Nevertheless, it has limited practical applications due to it could only respond to photons with wavelength in UV range and short photogenerated electron-hole pair lifetimes.[3] Therefore, it is very urgent and critical to develop efficient, sustainable and stable visible-light-active photocatalysts. Up to now, many attempts have been paid to prepare novel visible-light-driven photocatalysts with high efficiency.[4] Among them, graphitic carbon nitride (g-C_3N_4), as a metal-free polymeric semiconductor material, which manifests high visible-light photocatalytic activity for hydrogen or oxygen production from water splitting under visible light irradiation, because its good thermal and chemical stability, tunable electronic structure, good biocompatibility, cheap and responsiveness to visible light.[4d,5] Unfortunately, the photocatalytic performance of g-C_3N_4 is still limited due to the high recombination rate of the photo-generated charge carriers.[6] Furthermore, the weak van der Waals interaction between adjacent conjugated planes also hinders the electron coupling between the planes that negatively affect the electron transfer and photocatalytic activity.[7] To address these limitations, numerous efforts have been made to improve the photocatalytic performance of g-C_3N_4, including doping metal or nonmetal element,[8] noble metal deposition,[9] optimizing porous structure and coupling with other semiconductors.[10] Among them, doping is proven to be an effective method for improving the photocatalytic activity of g-C_3N_4, due largely to widen optical absorption range,[8a] enhanced dye and optical absorption and accelerated charge carriers transfer rate.[11] Additionally, g-C_3N_4 coupled with other semiconductor materials to form g-C_3N_4-based composites, such as Co_3O_4/g-C_3N_4,[3b] MoS_2/g-C_3N_4,[12] $BiVO_4$/g-C_3N_4,[13] Ag_3PO_4/g-C_3N_4,[14] $HSbO_3$/g-C_3N_4,[15] Ag_2CO_3/g-C_3N_4,[16] is another effective strategy for improving the photocatalytic activity potentially attributed to improving charge separation and enhancing visible light absorption. However, to the best of our knowledge, few literatures on the property and photocatalytic performance of both doping and coupling with g-C_3N_4 were reported.

Hence, in this study, inspired by doping and coupling with other semiconductors to improve the photocatalytic activity of g-C_3N_4, we deliberately designed a novel g-C_3N_4-based composite photocatalyst composed of phosphorus doped g-C_3N_4 (P-C_3N_4) and CeO_2. First of all, P-C_3N_4 catalyst was prepared via a facile one-pot method by simply heating the

School of Chemistry and Chemical Engineering, Institute of Physical Chemistry, and Development Center for New Materials Engineering & Technology in Universities of Guangdong, Lingnan Normal University, Zhanjiang 524048, China. E-mail: lj328520504@126.com; Tel/Fax: +86-759-3183205

mixture of melamine and diammonium hydrogen phosphate as g-C_3N_4 precursors and P source under 550 ^oC, respectively. Then, CeO_2 nanoparticles coupled with P-C_3N_4 composite photocatalysts (CeO_2/P-C_3N_4) via a facile mixing-calcination route. The photocatalytic activity and stability of CeO_2/P-C_3N_4 photocatalysts were evaluated in the photocatalytic degradation of methyl orange (MO) under visible light irradiation (λ>420 nm). The experimental results showed that the as-prepared CeO_2/P-C_3N_4 composites predominantly enhanced photocatalytic activity compare with that over pure g-C_3N_4 and CeO_2. The activity enhancement was mainly ascribed to the synergetic effect between P-C_3N_4 and CeO_2, which was found to extend the visible light absorption range, enhance visible light absorption and improve photogenerated electron-hole pairs separation efficiency after doping phosphorus and coupling with CeO_2. Moreover, a possible photocatalytic process for enhancing photocatalytic activity over CeO_2/P-C_3N_4 composites was proposed.

Experimental

Catalysts synthesis

P-C_3N_4 catalyst was prepared via a facile one-pot method by simply heating the mixture of melamine and diammonium hydrogen phosphate ($(NH_4)_2HPO_4$) according to a modified reported procedure.[17] Typically, 3 g melamine was dispersed in 20 mL of deionized water and stirred for 30 min, then 0.35 g $(NH_4)_2HPO_4$ was added into the above suspension and stirred for 30 min, then further stirred at room temperature for 5 h. The obtained solution was heated to 100 ^oC to remove the water. The solid product was dried at 110 ^oC for 6 h in oven, followed by milling and annealing at 550 ^oC in a muffle furnace for 4 h in a semiclosed system at a heating rate of 20 ^oC min^{-1} under air condition. The as-prepared sample was denoted as P-C_3N_4. For comparison, g-C_3N_4 photocatalyst was prepared following the same procedure mentioned above in the absence of $(NH_4)_2HPO_4$.

CeO_2/P-C_3N_4 composite photocatalysts were prepared by a facile mixing-calcination route as follows: typically, three copies of 500 mg as prepared P-C_3N_4 samples were immersed into 20 mL Ce^{3+} solutions with different amounts of $Ce(NO_3)_3{\cdot}6H_2O$ (i.e., 100, 200 and 300 mg) added in, respectively. The suspensions were stirred at room temperature for 5 h. The obtained solution was heated to 100 ^oC to remove the water. The solid product was dried at 110 ^oC for 6 h in oven, followed by milling and annealing at 500 ^oC in a muffle furnace for 2 h in a semiclosed system at a heating rate of 20 ^oC min^{-1} under air condition. The obtained products were denoted as CeO_2(x%)/P-C_3N_4, where x% stands for the mass percent of CeO_2 in CeO_2/P-C_3N_4. That is to say, the as-prepared samples were also denoted as CeO_2(7.4%)/P-C_3N_4, CeO_2(13.8%)/P-C_3N_4, and CeO_2(19.4%)/P-C_3N_4, respectively. For comparison, CeO_2 nanoparticles were prepared following the same procedure mentioned above in the absence of P-C_3N_4. In addition, CeO_2/g-C_3N_4 composite photocatalysts were prepared following the same procedure mentioned above except for P-C_3N_4 replacing by g-C_3N_4.

Catalysts characterization

X-ray diffraction (XRD) patterns of the as-prepared samples were recorded on an X-ray diffractometer (D/max-IIIA, Japan) using Cu K_a radiation. The surface morphology of as-prepared samples was examined by a scanning electron microscopy (SEM) (LEO1530VP, LEO Company) and a transmission electron microscope (TEM, JEOL, JEM2100). The UV-Vis light absorption spectra of as-prepared samples were obtained from a Hitachi UV-3010 spectrophotometer equipped with an integrating sphere assembly and using the diffuse reflection method and $BaSO_4$ as a reference to measure all the samples. The each of the chemical nature elements in the CeO_2/P-C_3N_4 has been studied using X-ray photoelectron spectroscopy (XPS) in Krato Axis Ultra DLD spectrometer. The binding energy was referenced to C1s line at 284.6 eV for calibration. Photoluminescence (PL) spectra were measured on an F-7000 Fluorescence spectrohpotometer (Hitachi, Japan).

Photocatalytic tests of catalysts

The photocatalytic performance of the samples was evaluated through the photodegradation of MO under visible light. A 500 W Xe-arc lamp equipped with a 420 nm cutoff filter was used as a visible light source. In a typical photocatalytic measurement, suspension including the photocatalyst (50 mg) and MO solution (150 mL, 10 mg L^{-1}) was laid in a 250 mL cylindrical quartz reactor equipped with a water circulation facility. Before irradiation, the reaction suspension was ultrasonicated for 5 min and stirred in the dark for 60 min to ensure the equilibrium of adsorption and desorption. During the photocatalytic tests, 5 mL of the suspension was obtained at a given time intervals, followed by centrifugation at 10000 rpm for 10 min to remove the photocatalyst. The concentration of the remaining MO was measured by its absorbance (A) at 465 nm with a Hitachi UV-3010 spectrophotometer. The degradation ratio of MO can be calculated by $X=(A_0-A_t)/A_0\times100\%$, where A_0 and A_t are the concentration of MO before illumination and after illumination time t.

Results and discussion

Fig. 1 shows the SEM and TEM images of the as-synthesized photocatalysts. As shown in Fig. 1a, the morphology of g-C_3N_4 seems to be smooth, and the layer structure might be the origin of the special morphology of g-C_3N_4. It is noted that the morphology of P-C_3N_4 seems also to be smooth (Fig. 1b), indicating the layer structure is not changed after phosphorus doping. Fig. 1f shows an image of CeO_2 composed of a large number of irregular and agglomerated nanoparticles. Fig. 1c shows amounts of CeO_2 irregular nanoparticles are deposited on the smooth surfaces of P-C_3N_4. Moreover, CeO_2 samples mainly consist of 10-20 nm particles, and they are highly dispersed on the surfaces of P-C_3N_4 (Fig. 1d). It is consistent with the SEM observation. Furthermore, it can be further confirmed from the elemental mapping images of

CeO_2(13.8%)/P-C_3N_4 (Fig. S1). As shown in Fig. S1, the Ce and O elements are homogenously distributed in the whole host of CeO_2(13.8%)/P-C_3N_4 composite. Similarly, the Ce and O elements are also homogenously distributed in the whole host of CeO_2(13.8%)/g-C_3N_4 composite (Fig. S2). These studies confirm that P-C_3N_4 or g-C_3N_4 could serve as a support to bound CeO_2 particles in this composite system. On the other side, the as-prepared CeO_2(13.8%)/P-C_3N_4 composite is purely composed of CeO_2 and P-C_3N_4, it can be confirmed from the energy dispersive X-ray spectrum (EDS) of CeO_2(13.8%)/P-C_3N_4 (Fig. S3). As shown in Fig. S3b, it can be unambiguously seen that the CeO_2(13.8%)/P-C_3N_4 composite contains only C, N, P, Ce and O elements and no other element or impurity found, demonstrating that CeO_2(13.8%)/P-C_3N_4 composite was only composed of both CeO_2 and P-C_3N_4. Moreover, it is noted that the mass percent of P in the CeO_2 (13.8%)/P-C_3N_4 composite was determined to be 3.6 %, and P content in pristine the P-C_3N_4 and CeO_2(13.8%)/P-C_3N_4 composite was unchanged obviously (Fig. S3).

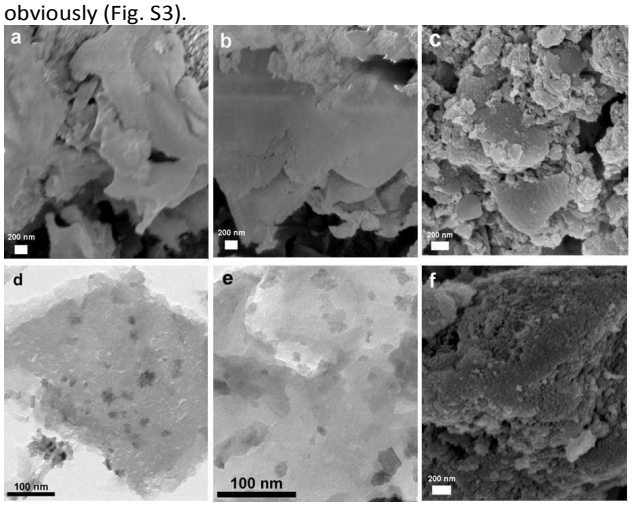

Fig. 1 SEM (a, b, c and f) and TEM (d and e) images of g-C_3N_4 (a), P-C_3N_4 (b), CeO_2(13.8%)/P-C_3N_4 (c and d), CeO_2(13.8%)/P-C_3N_4 used for 4th cycle (e) and CeO_2 (f).

Fig. 2a shows the XRD patterns of g-C_3N_4, P-C_3N_4, CeO_2 and CeO_2/P-C_3N_4 series of composite photocatalysts. The results showed that all the as-prepared photocatalysts are crystalline. Pure g-C_3N_4 displays two distinct peaks at 2θ=13.0° and 27.4°, which are in good agreement with the (001) and (002) diffraction planes of the hexagonal phase of the graphite-like carbon nitride (JCPDS 87-1526).[3b] It is noted that no peak for phosphorus species was observed in the P-C_3N_4. More interestingly, compared with g-C_3N_4, a slight shift toward a higher 2θ (27.6°) value is observed for P-C_3N_4. This phenomenon is consistent with previous results.[18] Pure CeO_2 shows four distinct peaks at 2θ=28.6°, 33.2°, 47.5°, and 56.5°, which are in good agreement with the (111), (200), (220) and (311) diffraction planes of cubic fluorite CeO_2 (JCPDS 34-0349).[19] Moreover, the XRD patterns of CeO_2/P-C_3N_4 composites demonstrate characteristic diffraction peaks of both P-C_3N_4 and CeO_2 crystalline phases. However, compare with pure CeO_2, a slight shift toward a lower 2θ value is observed for all the CeO_2/P-C_3N_4 composites. This is probably due to the existence of interaction between CeO_2 and P-C_3N_4 in calcination process. It is noted that the diffraction intensity of the peak at 27.6° become gradually weaker with the increasing CeO_2 content, which indicate that the crystalline structure of P-C_3N_4 was probably damaged by the decomposition of nitrates usually generates a massive amount of heat. On the other side, the diffraction intensity of the peak at 28.6° increased gradually with the increasing CeO_2 content in the composite.

In order to identify the chemical status of the elements in as synthesized photocatalysts, CeO_2(13.8%)/P-C_3N_4 composite is characterized by XPS spectra (Fig. 2b-f). High resolution XPS spectra of C1s, O1s, N1s, P2p and Ce3d were shown in Fig. 2b-f. For the C1s, two peaks can be distinguished at 284.6 and 288.0 eV, which are attributed to the pure graphitic species in the CN matrix and C-N-C coordination in graphitic carbon nitride,[3b,10b] respectively, while another extra C1s peak located at 289 eV is attributed to the O-C=O.[20] For the O1s, the peak at 530.8 eV is attributed to the O^{2-} anion,[10b] while the other O1s peak at 531.9 eV because of the formation of O-H bonds.[21] For the N1s, the main N 1s peak at a binding energy of 398.7 eV can be assigned to sp^2 hybridized nitrogen (C=N-C), confirming the presence of sp^2-bonded graphitic carbon nitride, while the peak at higher binding energy 400.5 eV is attributed to tertiary nitrogen N-$(C)_3$ groups.[22] For the P2p, the peak at 133.0 eV and 133.8 eV are attributed to the P-N bond.[17,18,20a,23] thus it is deduced that phosphorus doped into g-C_3N_4 lattice in the formation of P-N bond. For the Ce3d, both 3+ and 4+ states are present in CeO_2(13.8%)/P-C_3N_4 composite. The main peaks of $Ce^{3+}3d_{3/2}$ and $Ce^{3+}3d_{5/2}$ are shown at the binding energies of 904.5 ev and 886.0 ev, respectively, while three additional peaks of $Ce^{3+}3d_{5/2}$, $Ce^{3+}3d_{3/2}$ and $Ce^{4+}3d_{3/2}$ at are located at 882.4 ev, 900.7 ev and 916.7 ev,[19b,24] respectively. Therefore, with the combination of the XRD, EDS, TEM and XPS investigation, the results confirm that there are both CeO_2 and P-C_3N_4 species in the CeO_2/P-C_3N_4 composite.

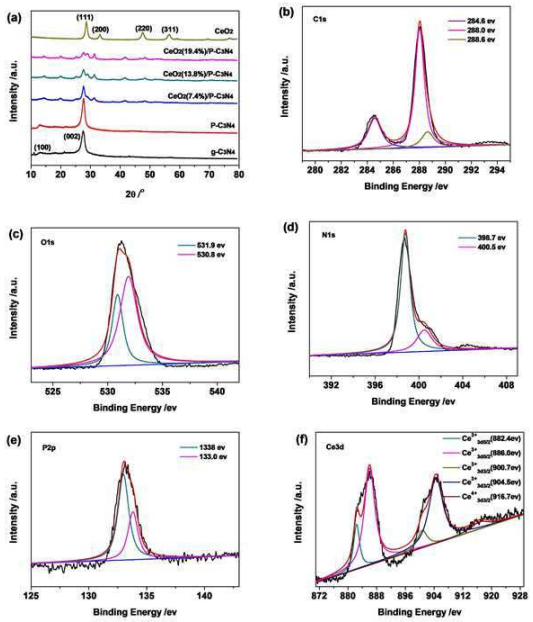

Fig. 2 XRD patterns (a) of the as-prepared photocatalysts, C1s (b), O1s (c), N1s (d), P2p (e) and Ce3d (f) XPS spectrum of the CeO_2(13.8%)/P-C_3N_4 photocatalyst.

The synergetic effect of P-C_3N_4 and CeO_2 on the light sorption properties was investigated, which may play a critical role in determining the photocatalytic performance, especially for the visible light photodegradation of contaminants. The absorbance of the as-prepared samples was measured by UV-vis diffuse reflection spectra (UV-vis DRS), and the results are recorded in Fig.3. As shown in Fig. 3A, the band gap absorption edge of CeO_2 is around 440 nm. Moreover, the g-C_3N_4 sample has photo-absorption from UV light to visible light, and the wavelength of the absorption edge is around 456 nm, originating from charge transfer response of g-C_3N_4 from the VB populated by N2p orbital to the CB formed by C2p orbital.[4d,25] Interestingly, in comparison with g-C_3N_4, there is a slight red shift in the absorption edge and an improved absorbance in the visible light region ranging from 450 to 800 nm after phosphorus doping, indicating phosphorus doping changed the optical property of g-C_3N_4. More interestingly, the absorption intensities of all the CeO_2/P-C_3N_4 samples were shown a significant enhancement at the wavelength range of 450-800 nm compared with P-C_3N_4 and CeO_2, which might be due to the existence of interaction between P-C_3N_4 and CeO_2. It effectively decreased the contact barrier and strengthen the electronic coupling of P-C_3N_4 and CeO_2, leading to the strong light absorption of CeO_2/P-C_3N_4 composites at longer wavelengths. On the other side, some formed chemical bonds between the two semiconductors might result in the promoted optical property, similar as that in ZrO_2/g-C_3N_4 composites.[26] The band gap energy of as-prepared samples can be calculated through the equation $\alpha hv=A(hv-E_g)^{n/2}$.[19b,27] where A, α, v, E_g and h are a constant, absorption coefficient, light frequency, band gap energy and Planck constant, respectively. For the value of n, it was determined by the type of optical transition of semiconductors (n=1 for direct transition and n=4 for indirect transition). For CeO_2 and g-C_3N_4, the values of n are 1 and 4, respectively.[27,28] Accordingly, as shown in Fig. 3B, the band gap energy of CeO_2 is estimated to about 2.80 eV according to a plot of $(\alpha hv)^2$ versus energy (hv). On the other side, according to plots of $(\alpha hv)^{1/2}$ versus energy (hv), the band gap energies of the g-C_3N_4 and P-C_3N_4 are estimated to about 2.71 eV and 2.62 eV, respectively, indicating phosphorus doping decreased the band gap energy. It is noteworthy that the band gap energies of the CeO_2/P-C_3N_4 composites, which is from 2.62 ev gradually decreased to 2.32 ev with increasing CeO_2 content, clearly indicating that the absorption of CeO_2/P-C_3N_4 composite photocatalysts is shifted to the lower energy region, which might be due to the interaction between CeO_2 and P-C_3N_4. That is, the synergistic effect between CeO_2 and P-C_3N_4 effectively enhanced the separation of electron-hole pairs account for the band gap transition of photo-generated electrons and then enhanced the absorption in the visible light region, similar as that in $BiPO_4$/g-C_3N_4 and ZrO_2/g-C_3N_4 composites.[26,29]

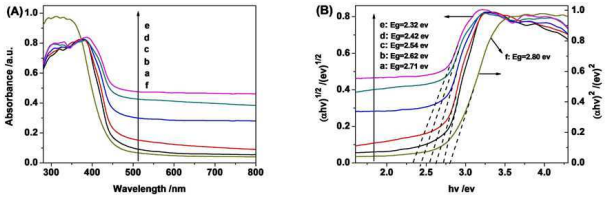

Fig. 3 UV-vis DRS (A) and plots of $(\alpha hv)^{1/2}$ vs. photon energy (B) of g-C_3N_4 (a), P-C_3N_4 (b), CeO_2(7.4%)/P-C_3N_4 (c), CeO_2(13.8%)/P-C_3N_4 (d), CeO_2(19.4%)/P-C_3N_4 (e) and plot of $(\alpha hv)^2$ vs. photon energy (B) of CeO_2(f).

The photoluminescence (PL) emission spectra is usually employed to investigate the migration, transfer and recombination processes of photo-generated charge carriers in semiconductors,[16,30] which play a crucial role in photocatalytic reactions. Generally, the lower PL intensity, the lower recombination rate of photoinduced electron-hole pairs, thus the higher photocatalytic activity. Fig. 4a exhibits the PL spectra of as-prepared samples under the excitation wavelength of 325 nm, and all the catalysts exhibit similar PL spectra. The PL spectra of g-C_3N_4 exhibits a strong emission band centered at about 450 nm, which was attributed to the recombination process of self-trapped excitations.[31] Obviously, g-C_3N_4 shows the higher PL intensity than that of other photocatalysts, indicating g-C_3N_4 has the highest optical recombination rate that deteriorated the photodegradation efficiency. Notably, the emission intensity of the PL spectra for the g-C_3N_4, P-C_3N_4 and CeO_2/P-C_3N_4 composites significantly decreases. Interestingly, the P-C_3N_4 exhibits more quenching of the PL emission compared to g-C_3N_4, indicating that phosphorus doping leads to superior separation of the electron-hole pairs. Besides, the PL emission intensity of P-C_3N_4 obviously decreased after the addition of CeO_2 species, indicating that the recombination of electron-hole pairs is efficiently prevented by CeO_2 modification. The stronger interaction between P-C_3N_4 and CeO_2 may cause the better electrons-holes separation efficiency, which results in higher photodegradation efficiency. It is noted that the CeO_2(13.8%)/P-C_3N_4 composite has the lowest recombination rate of photogenerated charge carriers compared with other composites, suggesting that the CeO_2(13.8%)/P-C_3N_4 photocatalyst would have the highest photocatalytic activity, which is mainly due to the fact that the excited electrons of conduction band from the valence band of P-C_3N_4 are then transfer to the conduction band of CeO_2, preventing a direct recombination of electron-hole pairs. Thus, the greatest separation of photogenerated charge carriers contributes to the enhanced photocatalytic activity of CeO_2(13.8%)/P-C_3N_4. However, when CeO_2 content further increased to 19.4%, the PL emission intensity of CeO_2(19.4%)/P-C_3N_4 obviously increased, suggesting that the CeO_2(19.4%)/P-C_3N_4 composite has a higher recombination rate of photogenerated charge carriers compared with CeO_2(13.8%)/P-C_3N_4, leading to inferior separation of the electron-hole pairs, arising from the excess

CeO_2 species may act as a recombination centre and thereby reducing the efficiency of charge separation.

The photocatalytic activities of the as-prepared samples were evaluated by the degradation of MO under visible light irradiation (λ≥420 nm), as shown in Fig. 4b-d. As expected, the blank test shows that MO is stable under visible light irradiation, indicating that the photolysis of MO is almost negligible in the absence of photocatalyst, and MO is degraded via photocatalytic process. MO degrades very slowly in the presence of CeO_2 or g-C_3N_4 under visible light irradiation, which only 10% or 15% MO is photodegraded after irradiated for 2h, respectively. Interestingly, 24% MO is photodegraded after irradiated for 2h in the presence of P-C_3N_4, which is 1.6 times higher than that of g-C_3N_4, indicating that phosphorus doping efficiently enhanced the photocatalytic activity of g-C_3N_4, arising from enhancing visible light absorption and improving electrons-hole pairs separation efficiency. More interestingly, the photocatalytic performance of P-C_3N_4 is greatly enhanced after modification by CeO_2 species, indicating that CeO_2 play an important role in the enhancement of MO degradation. It is worth mentioning that the photocatalytic activity increases first and then decreases with the increasing content of CeO_2 species. When the weight ratio of CeO_2 increased to 13.8%, the CeO_2(13.8%)/P-C_3N_4 composite photocatalyst exhibited the highest photocatalytic activity, in other words, 74% MO is photodegraded after irradiated for 2h in the presence of CeO_2(13.8%)/P-C_3N_4, which is 4.9 and 7.4 times higher than that of pure g-C_3N_4 and CeO_2. It may be the suitable CeO_2 species can form a good dispersion on the P-C_3N_4 surfaces, which favored the separation and transfer of the charge carriers. These results clearly revealed that both doping phosphorus and coupling with CeO_2 species are proven to be an effective method for improving the photocatalytic activity of g-C_3N_4. However, when the CeO_2 content further increased to 19.4%, there was a decrease in photocatalytic activity under the same conditions, but it was much higher compared to the photocatalytic activity of pure P-C_3N_4 and CeO_2, which indicates that excess CeO_2 species had a negative effect on the photocatalytic activity. This can be attributed to the possibility that the excess CeO_2 species may act as a recombination centre, and cover the active sites on the P-C_3N_4 surface and thereby reducing the efficiency of charge separation and decreasing the intensity of light through the depth of the reaction solution. Consequently, a suitable content of CeO_2 species is crucial for optimizing the photocatalytic performance, due to the significant synergistic effect between P-C_3N_4 and CeO_2 for the photodegradation of MO under visible light irradiation. Furthermore, for comparison purposes, we also conducted the CeO_2(13.8%)/g-C_3N_4 composite for the photodegradation of MO under identical conditions, whereas only 35% MO is photodegraded after irradiated for 2h, which is much lower than that of the CeO_2(13.8%)/P-C_3N_4 composite (Fig. S4a). It may be due to the former has a lower the visible light absorption intensity and a higher recombination rate of photogenerated charge carriers compared with the latter (Fig. S5 and S6).

To quantitatively investigate the reaction kinetics of the MO degradation, the experimental data were fitted by applying a first-order model as expressed by the formula: $-ln(C/C_o)=kt$. where C_o is the equilibrium concentration of MO after 60 min dark adsorption, C is the MO concentration remaining in the solution at irradiation time t (min), and k is the apparent first-order rate constant.[32] As shown in Fig. 4c, the plots of $-ln(C/C_o)$ against the irradiation time (t) are nearly linear, and thus the corresponding the apparent first-order rate constants (k) were calculated. As shown in Fig. 4d, the apparent first-order rate constants (k) for MO degradation with CeO_2, g-C_3N_4, P-C_3N_4, CeO_2(7.4%)/P-C_3N_4, CeO_2(13.8%)/P-C_3N_4 and CeO_2(19.4%)/P-C_3N_4 were estimated to be 0.0009min^{-1}, 0.0014min^{-1}, 0.0022min^{-1}, 0.0074min^{-1}, 0.0110min^{-1} and 0.0087min^{-1}, respectively. Remarkably, the rate constant of the CeO_2(13.8%)/P-C_3N_4 composite is 12.2 times as high as that of pure CeO_2 and 7.9 or 5.0 times larger than that of pure g-C_3N_4 or P-C_3N_4 under the same experimental conditions. Additionally, it is noteworthy that the rate constant of the CeO_2(13.8%)/P-C_3N_4 composite is 3.0 times larger than that of CeO_2(13.8%)/g-C_3N_4 composite under the same experimental conditions (Fig. S4b). These results clearly indicated both doping phosphorus and coupling with CeO_2 could dramatically enhance the photocatalytic capability of g-C_3N_4 under the visible light irradiation. Consequently, the CeO_2(13.8%)/P-C_3N_4 composite is the best performing sample and was selected for the following recycling experiments.

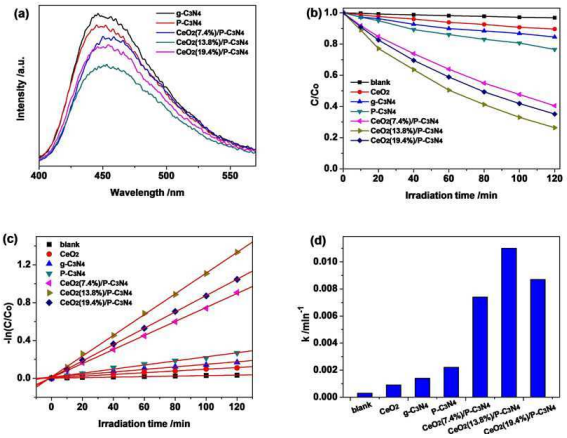

Fig. 4 PL spectra (a) of as-prepared photocatalysts, photocatalytic activities (b) of as-prepared photocatalysts for the photodegradation of MO in aqueous solution under visible light irradiation (λ≥420 nm), first-order kinetics plot (c) and the kinetic constants (d) for the photodegradation of MO in aqueous solution over as-prepared photocatalysts.

The stability of a photocatalyst is very important from point of view of its practical application. To evaluate the stability of the composite catalysts, recycling reactions were carried out for the photodegradation of MO over CeO_2(13.8%)/P-C_3N_4 photocatalyst under visible light irradiation. After each run, the recycled catalyst was separated from the aqueous suspension by centrifugation, repeatedly washed by deionized water and ethanol and dried in vacuum at 100 ^{o}C for 12h. As can be seen from Fig. 5a, the photodegradation of MO in every cycling runs, and there was slight catalyst deactivation in the fourth run, but the photocatalytic activity of CeO_2(13.8%)/P-C_3N_4 was retained at over 80% of its original activity after four successive experimental runs, arising from the slight loss of photocatalyst during the cycling reaction. In addition, as shown in Fig. 1e, Fig. 5b and 5c, after four consecutive cycles, the morphology, XRD

patterns and FT-IR curves of the CeO_2(13.8%)/P-C_3N_4 composite are all unchanged obviously, clearly suggest that the CeO_2(13.8%)/P-C_3N_4 composite photocatalyst can be regarded as stable during the photocatalytic degradation of MO under visible light irradiation.

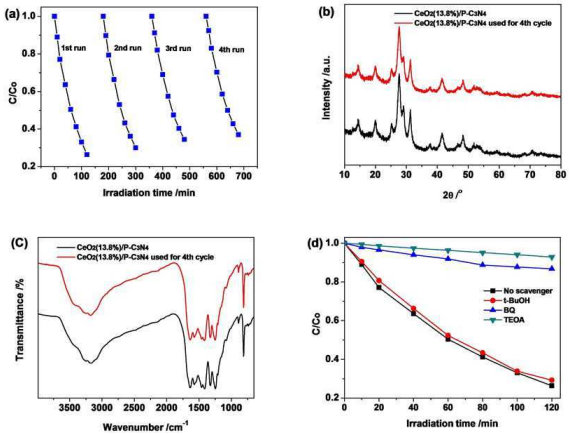

Fig. 5 Recyclability (a) of the CeO_2(13.8%)/P-C_3N_4 composite catalyst in four successive experiments for the photocatalytic degradation of MO in aqueous solution under visible light irradiation, XRD patterns (b) and FT-IR curves (c) of the CeO_2(13.8%)/P-C_3N_4 composite catalyst before and after four consecutive photocatalytic reactions, effects of various scavengers (d) on the visible light photocatalytic activity of CeO_2(13.8%)/P-C_3N_4 composite.

To understand the reaction mechanism, it is important to identify the active species that participate in the photocatalytic process. The active species generated during the reaction process are identified by hole and free radical trapping experiment. In this investigation, tert-butyl alcohol (t-BuOH), triethanolamine (TEOA) and 1,4-benzoquinone (BQ) are used as hydroxyl radical (•OH), hole (h^+) and superoxide radical ($\bullet O_2^-$) scavenger, respectively.[22b,33] As illustrated in Fig. 5d, after the addition of t-BuOH, the photocatalytic activity of the CeO_2(13.8%)/P-C_3N_4 composite decreases slightly compared to that without scavengers, indicating that •OH is not the main active species in CeO_2(13.8%)/P-C_3N_4 photocatalytic systems. On the contrary, once TEOA or BQ is added, the photocatalytic activity of the CeO_2(13.8%)/P-C_3N_4 composite decreases significantly, meaning that h^+ and $\bullet O_2^-$ are the principle oxidative species that participate in the photodegradation reaction.

The conduction band (CB) potentials of a semiconductor can be determined using the empirical equation: $E_{CB}=X-E^C-0.5E_g$, where X is the absolute electronegativity of the semiconductor (the X values for CeO_2 and g-C_3N_4 are 5.56 eV,[34] and 4.72 eV,[35] respectively), E^C is the energy of free electrons on the hydrogen scale (about 4.5 eV vs. NHE) and E_g is the band gap of the semiconductor.[34,36] Moreover, The valence band (VB) potentials can be obtained by $E_{VB}=E_{CB}+E_g$. Based on the result in the Fig. 3B, the band gap energies of CeO_2 and g-C_3N_4 were estimated at 2.80 eV and 2.71 ev, respectively. Thus the calculated VB and CB potentials of CeO_2 are 2.46 eV (EVB) and -0.34 eV (ECB), respectively, while the calculated VB and CB potentials of g-C_3N_4 are 1.57 eV and -1.14 eV, respectively. Additionally, according to the previous report,[37] P doping induced a downshifting of the CB edge of g-C_3N_4, while almost without altering the VB edge owing to the absolute electronegativity of P is smaller than those of both N and C. Consequently, the calculated VB and CB potentials of P-C_3N_4 were estimated at 1.57 eV and -1.05 eV, respectively.

On the basis of the above-mentioned experimental results and analysis, the schematic mechanism of the photocatalytic activity of the CeO_2(13.8%)/P-C_3N_4 composite photocatalyst is proposed and illustrated in Fig. 6. Under the irradiation of visible light, both P-C_3N_4 and CeO_2 can be both excited and generate the photoinduced electron-hole pairs (eqn (1) and (2)). Then the photoinduced electrons on the P-C_3N_4 surfaces get easily transferred to the CB of CeO_2 (eqn (3)) due to the fact that the CB edge potential of P-C_3N_4 is more negative than that of CeO_2, while the holes on the VB of CeO_2 could transfer to the VB of P-C_3N_4 through the closely contacted interfaces (eqn (4)). More importantly, the migration of photoinduced charge carriers can be promoted by the inner electric field established at the heterojunction interface.[38] Therefore, the photogenerated electron-hole pairs can be efficiently separated due to the synergistic effect between P-C_3N_4 and CeO_2, inducing more charge carriers to participate in photodegradation process, further resulting in the enhanced photocatalytic activity. Additionally, the enriched electrons left on the CB of CeO_2 could be trapped by dissolved oxygen in the reaction solution to form $\bullet O_2^-$ (eqn (5)) due to the CB (-0.34 ev) of CeO_2 is lower than $E(O_2/\bullet O_2^-)$ (0.13 ev vs. NHE),[6] subsequently, produced $\bullet O_2^-$ would oxidize the MO to CO_2, H_2O and other inorganic molecules, while the holes located on the VB of P-C_3N_4 would also oxidize the MO directly to CO_2, H_2O and other inorganic molecules (eqn (6)). This is consistent with our experiment results, the MO degradation rate is decreased obviously in the presence of TEOA or BQ. The process is detailedly described as follows:

$$\text{P-}C_3N_4 + hv \rightarrow \text{P-}C_3N_4\,(e^-) + \text{P-}C_3N_4\,(h^+) \quad (1)$$

$$CeO_2 + hv \rightarrow CeO_2\,(e^-) + CeO_2\,(h^+) \quad (2)$$

$$\text{P-}C_3N_4\,(e^-) \rightarrow CeO_2\,(e^-) \quad (3)$$

$$CeO_2\,(h^+) \rightarrow \text{P-}C_3N_4\,(h^+) \quad (4)$$

$$CeO_2\,(e^-) + O_2 \rightarrow \bullet O_2^- \quad (5)$$

$$\bullet O_2^-, h^+ + MO \rightarrow CO_2 + H_2O + \text{other inorganic molecules} \quad (6)$$

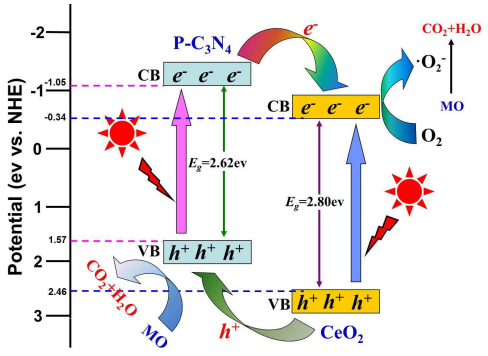

Fig. 6 Schematic illustration of the charge transfer pathway of the CeO_2/P-C_3N_4 composite catalyst under visible light irradiation.

Conclusions

In summary, highly efficient CeO_2/P-C_3N_4 composite photocatalysts have been successfully designed by doping phosphorus and coupling with CeO_2 species. More importantly, CeO_2/P-C_3N_4 composite exhibited the excellent photocatalytic activity for the photocatalytic degradation of methyl orange under visible light irradiation. Especially, the rate constant of the CeO_2(13.8%)/P-C_3N_4 composite is 12.2 times as high as that of pure CeO_2 and 7.9 times larger than that of pure g-C_3N_4, meaning that both doping phosphorus and coupling with CeO_2 species are proven to be an effective method for improving the photocatalytic activity of g-C_3N_4. The remarkable enhancement on photocatalytic performance was predominantly ascribed to the synergistic effect between P-C_3N_4 and CeO_2, which extended the visible light absorption range, enhanced visible light absorption and improved photogenerated electron-hole pairs separation efficiency after doping phosphorus and coupling with CeO_2. Additionally, the superoxide radical anions ($\bullet O_2^-$) and holes (h^+) were considered as the main reactive species during the photodegradation process, and a possible photocatalytic mechanism is proposed based on the experimental results. We believe the results presented here demonstrate a new opportunity for the design of more efficient visible-light-driven photocatalysts.

Acknowledgements

This research was supported by Lingnan Normal University Natural Science Foundation for the Ph.D. Start-up Program (ZL1308).

Notes and references

1 a) F. Fresno, R. Portela, S. Suárez, J.M. Coronado, *J. Mater. Chem. A*., 2014, **2**, 2863-2884; b) T. Hisatomi, J. Kubota, K. Domen, *Chem. Soc. Rev.*, 2014, **43**, 7520-7535.

2 a) R. Asahi, T. Morikawa, H. Irie, T. Ohwaki, *Chem. Rev.*, 2014, **114**, 9824-9852; b) L. Z. Wang, T. Sasaki, *Chem. Rev.*, 2014, **114**, 9455-9486; c) J. X. Qiu, S. Q. Zhang, H. J. Zhao, *Sens. Actuators B,* 2011, **160**, 875-890.

3 a) H. L. Wang, L. S. Zhang, Z. Q. Chen, J. Q. Hu, S. J. Li, Z. H. Wang, J. S. Liu, X. C. Wang, *Chem. Soc. Rev.*, 2014, **43**, 5234-5244; b) C. Han, L. Ge, C. Chen, Y. Li, X. Xiao, Y. Zhang, L. Guo, *Appl. Catal. B: Environ.*, 2014, **147**, 546-553.

4 a) Y. Z. Wang, S. Li, J. S. Han, W. Wen, H. Wang, S. Dimitrijev, S. Q. Zhang, *RSC Adv.*, 2014, **4**, 54441-54446; b) D. J. Martin, G. G. Liu, S. J. A. Moniz, Y. P. Bi, A. M. Beale, J. H. Ye, J. W. Tang, *Chem. Soc. Rev.*, 2015, DOI: 10.1039/C5CS00380F; c) H. F. Cheng, B. B. Huang, Y. Dai, *Nanoscale*, 2014, **6**, 2009-2026; d) X. C. Wang, K. Maeda, A. Thomas, K. Takanabe, G. Xin, J.M. Carlsson, K. Domen, M. Antonietti, *Nat. Mater.*, 2009, **8**, 76-80.

5 J. Liu, Y. Liu, N. Y. Liu, Y. Z. Han, X. Zhang, H. Huang, Y. Lifshitz, S. T. Lee, J. Zhong, Z. H. Kang, *Science*, 2015, **347**, 970-974.

6 S. Kumar, T. Surendar, A. Baruah, V. Shanker, *J. Mater. Chem. A*, 2013, **1**, 5333-5340.

7 L. Xu, W. Q. Huang, L. L. Wang, Z. A. Tian, W. Y. Hu, Y. M. Ma, X. Wang, A. L. Pan, G. F. Huang, *Chem. Mater.*, 2015, **27**, 1612-1621.

8 a) X. F. Chen, J. S. Zhang, X. Z. Fu, M. Antonietti, X. C. Wang, *J. Am. Chem. Soc.*, 2009, **131**, 11658-11659; b) G. Liu, P. Niu, C. H. Sun, S.C. Smith, Z. G. Chen, G.Q. Lu, H. M. Cheng, *J. Am. Chem. Soc.*, 2010, **132**, 11642-11648.

9 X. J. Bai, R. L. Zong, C. X. Li, D. Liu, Y. F. Liu, Y. F. Zhu, *Appl. Catal. B: Environ.*, 2014, **147**, 82-91.

10 a) X. C. Wang, K. Maeda, X. F. Chen, K. Takanabe, K. Domen, Y. D. Hou, X. Z. Fu, M. Antonietti, *J. Am. Chem. Soc.*, 2009, **131**, 1680-1681; b) Y. M. He, L. H. Zhang, X. X. Wang, Y. Wu, H. J. Lin, L. H. Zhao, W. Z. Weng, H. L. Wan, M. H. Fan, *RSC Adv.*, 2014, **4**, 13610-13619.

11 a) S. C. Yan, Z. S. Li, Z. G. Zou, *Langmuir*, 2010, **26**, 3894-3901; b) G. G. Zhang, M. W. Zhang, X. X. Ye, X. Q. Qiu, S. Lin, X. C. Wang, *Adv. Mater.*, 2014, **26**, 805-809.

12 L. Shi, L. Liang, F. X. Wang, M. S. Liu, J. M. Sun, *Energy and Environ. Focus*, 2015, **4**, 74-81.

13 N. Tian, H. W. Huang, Y. He, Y. X. Guo, T. R. Zhang, Y. H. Zhang, *Dalton Trans.*, 2015, **44**, 4297-4307.

14 S. G. Meng, X. F. Ning, T. Zhang, S. F. Chen, X. L. Fu, *Phys. Chem. Chem. Phys.*, 2015, **17**, 11577-11585.

15 C. L. Wen, H. T. Zhang, Q. B. Bo, T. Z. Huang, Z. L. Lu, Y. Wang, *Chem. Eng. J.*, 2015, **270**, 405-410.

16 Y. F. Li, L. Fang, R. X. Jin, Y. Yang, X. Fang, Y. Xing, S. Y. Song, *Nanoscale*, 2015, **7**, 758-764.

17 S. Z. Hu, L. Ma, J. Q. You, F. Y. Li, Z. P. Fan, G. Lu, D. Liu, J. Z. Gui, *Appl. Surf. Sci.*, 2014, **311**, 164-171.

18 S. Z. Hu, L. Ma, J. Q You, F. Y. Li, Z. P. Fan, F. Wang, D. Liu, J. Z. Gui, *RSC Adv.*, 2014, **4**, 21657-21663.

19 a) W. D. Cai, F. Chen, X. X. Shen, L. J. Chen, J. L. Zhang, *Appl. Catal. B: Environ.*, 2010, **101**, 160-168; b) L. Y. Huang, Y. P. Li, H. Xu, Y. G. Xu, J. X. Xia, K. Wang, H. M. Li, X. N. Cheng, *RSC Adv.*, 2013, **3**, 22269-22279.

20 a) Y. J. Zhou, L. X. Zhang, J. J. Liu, X. Q. Fan, B. Z. Wang, M. Wang, W. C. Ren, J. Wang, M. L. Li, J. L. Shi, *J. Mater. Chem. A*, 2015, **3**, 3862-3867; b) J. Luo, H. Yu, H. J. Wang, H. H. Wang, F. Peng, *Chem. Eng. J.*, 2014, **240**, 434-442.

21 S. N. Gu, W. J. Li, F. Z. Wang, S. Y. Wang, H. L. Zhou, H. D. Li, *Appl. Catal. B: Environ.*, 2015, **170**, 186-194.

22 a) X. J. Zou, Y. Y. Dong, Z. B. Chen, D. P. Dong, D. X. Hu, X. Y. Li, Y. B. Cui, *RSC Adv.*, 2015, **DOI:** 10.1039/C5RA01607J; b) Q. Zhang, H. Y. Wang, S. Z. Hu, G. Lu, J. Bai, X. X. Kang, D. Liu, J. Z. Gui, *RSC Adv.*, 2015, **5**, 42736-42743.

23 Y. J. Zhang, T. Mori, J. H. Ye, M. Antonietti, *J. Am. Chem. Soc.*, 2010, **132**, 6294-6295.

24 a) J. Chen, S. H. Shen, P. Wu, L. J. Guo, *Green Chem.*, 2015, **17**, 509-517; b) H. Li, G. F. Wang, F. Zhang, Y. Cai, Y. D. Wang, I. Djerdj, *RSC Adv.*, 2012, **2**, 12413-12423.

25 S. W. Cao, J. X. Low, J. G. Yu, M. Jaroniec, *Adv. Mater.*, 2015, **27**, 2150-2176.

26 X. X. Wang, L. H. Zhang, H. J. Lin, Q. Y. Nong, Y. Wu, T.H. Wu, Y. M. He, *RSC Adv.*, 2014, **4**, 40029-40035.

27 L. Wang, J. Ding, Y. Y. Chai, Q. Q. Liu, J. Ren, X. Liu, W. L. Dai, *Dalton Trans.*, 2015, **DOI:** 10.1039/C5DT01479D.

28 Y. Wang, Y. Di, M. Antonietti, H. R. Li, X. F. Chen, X. C. Wang, *Chem. Mater.*, 2010, **22**, 5119-5121.

29 X. J. Zou, Y. Y. Dong, Z. B. Chen, D. P. Dong, D. X. Hu, X.Y. Li, Y. B. Cui, *RSC Adv.*, 2015, DOI: 10.1039/C5RA01607J.

30 Y. M. He, L. H. Zhang, B. T. Teng, M. H. Fan, *Environ. Sci. Technol.*, 2015, 49, 649-656.

31 S. Tonda, S. Kumar, V. Shanker, *J. Environ. Chem. Eng.*, 2015, **3**, 852-861.

32 a) H. Xu, J. Yan, Y. G. Xu, Y. H. Song, H. M. Li, J. X. Xia, C. J. Huang, H. L. Wan, *Appl. Catal. B: Environ.*, 2013, **129**, 182-

193; b) S. Ye, L. G. Qiu, Y. P. Yuan, Y. J. Zhu, J. Xia, J. F. Zhu, *J. Mater. Chem. A*, 2013, **1**, 3008-3015.
33 S. W. Zhang, J. X. Li, X. K. Wang, Y. S. Huang, M. Y. Zeng, J. Z. Xu, *ACS Appl. Mater. Interfaces*, 2014, **6**, 22116–22125.
34 D. Channei, B. Inceesungvorn, N. Wetchakun, S. Ukritnukun, A. Nattestad, J. Chen, S. Phanichphant, *Sci. Rep.*, 2014, **4**, 5757.
35 K. Dai, L. H. Lu, C. H. Liang, G. P. Zhu, Q. Z. Liu, L. Geng, J. Q. He, *Dalton Trans.*, 2015, **44**, 7903-7910.
36 a) N. Wetchakun, S. Chaiwichain, B. Inceesungvorn, K. Pingmuang, S. Phanichphant, A.I. Minett, J. Chen, *ACS Appl. Mater. Interfaces*, 2012, **4**, 3718-3723; b) H. Xu, Y. G. Xu, H. M. Li, J. X. Xia, J. Xiong, S. Yin, C. J. Huang, H. L. Wan, *Dalton Trans.*, 2012, **41**, 3387-3394.
37 X. G. Ma, Y. H. Lv, J. Xu, Y. F. Liu, R. Q. Zhang, Y. F. Zhu, *J. Phys. Chem. C*, 2012, **116**, 23485-23493.
38 D. L. Jiang, L. L. Chen, J. J. Zhu, M. Chen, W. D. Shi, J. M. Xie, *Dalton Trans.*, 2013, **42**, 15726-15734.

Graphical Abstract

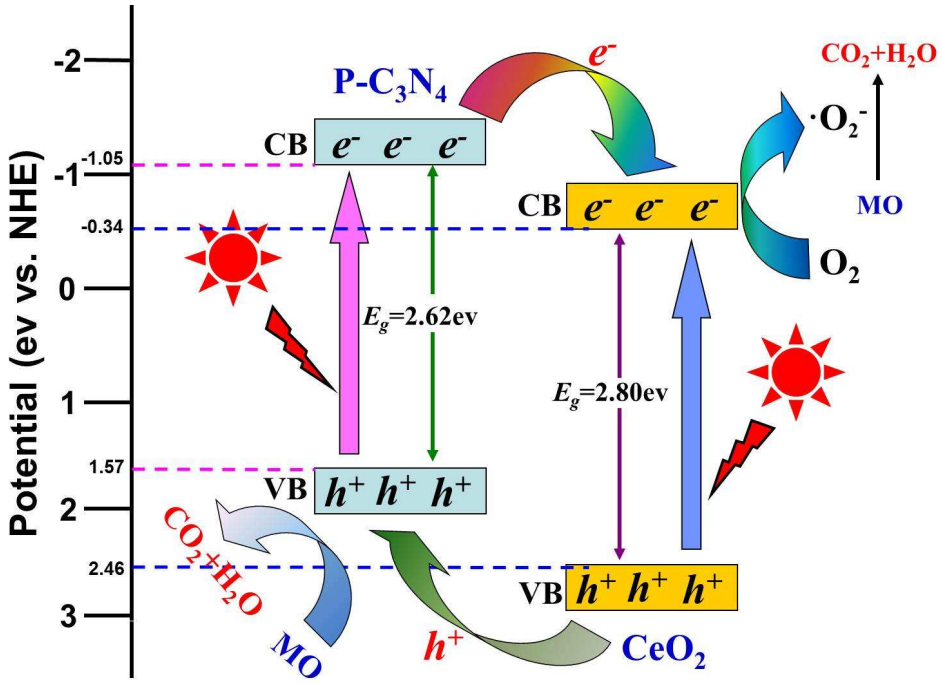

CeO_2/P-C_3N_4 composite catalysts exhibited excellent photocatalytic activity and stability for the photocatalytic degradation of methyl orange under visible light irradiation (λ>420nm), arising from the synergistic effect between P-C_3N_4 and CeO_2, which effectively improved photogenerated electron-hole pairs separation efficiency.